

# Phase Separation and Ripening in a Viscoelastic Material

Tine Curk<sup>1,\*</sup> and Erik Luijten<sup>1,2,†</sup>

<sup>1</sup>*Department of Materials Science & Engineering,  
Northwestern University, Evanston, Illinois 60208, USA*

<sup>2</sup>*Departments of Engineering Sciences & Applied Mathematics,  
Chemistry and Physics & Astronomy, Northwestern University, Evanston, Illinois 60208, USA*

(Dated: January 25, 2022)

The process of phase separation in elastic solids and viscous fluids is of fundamental importance to the stability and function of soft materials. We explore the dynamics of phase separation and domain growth in a viscoelastic material such as a polymer gel. Using analytical theory and Monte Carlo simulations we report a new domain growth regime, in which the domain size increases algebraically with a ripening exponent  $\alpha$  that depends on the viscoelastic properties of the material. For a prototypical Maxwell material, we obtain  $\alpha = 1$ , which is markedly different from the well-known Ostwald ripening process with  $\alpha = 1/3$ . We generalize our theory to systems with arbitrary power-law relaxation behavior and discuss our findings in the context of the long-term stability of materials as well as recent experimental results on phase separation in cross-linked networks and cytoskeleton.

## I. INTRODUCTION

Phase separation is a universal phenomenon and a fundamental concept in physics, chemistry and materials science. Whereas its outcome is described by equilibrium thermodynamics, it is equally important to understand the dynamics of the separation process. This is particularly relevant in solid, soft and biological systems where large kinetic barriers or active processes often prevent the system from reaching its equilibrium state. Upon formation of a new phase, domains typically grow via coalescence or via surface-tension-driven dissolution and redeposition known as Ostwald ripening [1]. However, elastic effects can markedly alter the dynamics of these processes. As shown in the early days of solid-state physics, nucleation and precipitation in crystalline solids cause substantial elastic stresses, which, in turn, control the shape and growth of precipitate particles and the macroscopic mechanical properties of the material [2]. Recent experiments on droplet formation within disordered polymer networks have shown that elastic stress can either arrest the coarsening process or inhibit liquid–liquid phase separation altogether [3, 4].

However, the situation is completely different in materials that exhibit viscoelastic relaxation or creep, which can irreversibly reduce elastic stress and thus enable further domain coarsening. Viscoelastic effects in phase separation have been extensively studied in spinodal decomposition [5], polymer solutions [6], viscoelastic fluids [7] and glass-forming melts [8–10], as well as in protein and colloidal suspensions [11]. However, to the best of our knowledge phase separation of a minority phase of small molecules inside a polymer matrix has only been studied on short timescales [3, 8], where coarsening is arrested by the elastic stress. In contrast, the long-time domain

growth of nuclei or droplets in a viscoelastic material and the associated coarsening laws are currently unknown. Consequently, a variety of material aging processes currently cannot be predicted.

This work was originally motivated by metal soap formation in oil paintings, an aging process believed to be driven by phase separation [12]. However, the relevance of our findings goes well beyond this topic, as it applies to various branches of materials science and is believed to play a crucial role in biological systems. Phase transitions involving biomolecular liquids have been established as fundamental drivers of intracellular organization [13, 14], and viscoelastic relaxation can enable cells to flexibly modulate mechanical properties of membraneless organelles [15, 16]. The realization that coupling between condensation and network elasticity may play a role in cellular physiology has led to renewed interest in phase separation in cells [17, 18] and in synthetic materials [3, 19].

Here, we employ analytical theory and particle-based Monte Carlo simulations to investigate the process of phase separation and surface-tension-driven coarsening within a viscoelastic medium. Focusing on a prototypical system where a minority phase forms spherical nuclei or droplets within a viscoelastic majority phase, we attain a fundamental and quantitative understanding of the coarsening process on both short and long timescales.

## II. PHASE SEPARATION IN ELASTIC MEDIA

To set the stage for our investigation of viscoelasticity, we first briefly introduce elastic effects in phase separation and coarsening. We limit our analysis to the dilute regime, so that many-body elastic effects can be neglected and each droplet or precipitate can be considered an isolated spherical inclusion in an isotropic elastic medium (Fig. 1a). The initial cavity size  $r_0$  is determined by the pore size in the material or the crosslink distance. For example,  $r_0^3 \sim k_B T / E_Y$  for a flexible gel

---

\* [curk@northwestern.edu](mailto:curk@northwestern.edu)

† [luijten@northwestern.edu](mailto:luijten@northwestern.edu)

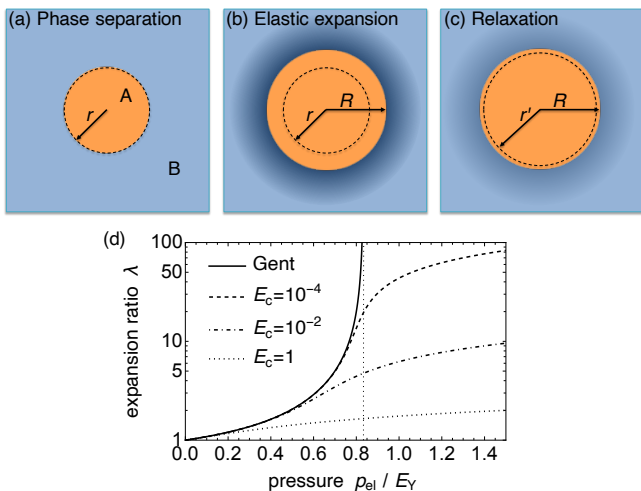


FIG. 1. Growth of a droplet in a viscoelastic medium. (a) Schematic of a minority phase A (orange) in an elastic majority phase B (blue), with  $r$  the unstressed cavity size. (b) Growth of the droplet to size  $R = \lambda r$  causes elastic stresses in phase B (indicated by a darker shade of blue). (c) Viscoelastic relaxation expands the cavity to size  $r'$ , thus reducing the stress and enabling further growth of phase A. (d) Droplet size dependence on pressure for a Gent material [Eq. (1)] (solid line) and for a material with additional nonlinear elasticity proportional to  $E_c$  (dashed, dot-dashed and dotted lines). The thin dotted vertical line indicates the elastic cavitation pressure  $p_c = 5E_Y/6$ .

with Young's modulus  $E_Y$  [20], with  $T$  the absolute temperature and  $k_B$  the Boltzmann constant. An inclusion of size  $R$  growing beyond the cavity size will produce a radial elastic stress in the majority phase B that is balanced by the excess pressure  $p_{el}$  within the inclusion (Fig. 1b). Viscoelastic relaxation can increase the cavity size, enabling further growth of the inclusion (Fig. 1c).

To describe the elastic expansion of the cavity we use the Gent model for a spherical inclusion in a rubber-like nonlinear solid [21, 22], a good approximation for cross-linked networks [3, 19, 23, 24],

$$p_{el}^{Gent}(\lambda) = \frac{E_Y}{6} \left( 5 - \frac{4}{\lambda} - \frac{1}{\lambda^4} \right), \quad (1)$$

with  $\lambda \equiv R/r$  the expansion ratio. At pressures exceeding the cavitation pressure  $p_c = 5E_Y/6$ , elastic forces are unable to contain the inclusion and its size  $R$  increases without bounds (Fig. 1d). However, it is known that additional nonlinear effects can limit the size at very high  $\lambda$  [3, 19, 23, 24]. We account for this through an additional term  $p_{el}^{lim} = E_c E_Y (\lambda - 1)^2$ , with dimensionless prefactor  $E_c > 0$ , that limits the expansion ratio to  $\lambda_c \sim E_c^{-0.5}$  [25]. We refer to this as the extended Gent model. On the other hand, at small deformations ( $\lambda \sim 1$ ) Eq. (1) reduces to  $p_e = \frac{4}{3}E_Y(\lambda - 1)$ , which corresponds to a standard result of linear elasticity,  $p_{el} = 2E_Y(\lambda - 1)/(1 + \nu)$  [26] with Poisson ratio  $\nu = 1/2$ . Thus, at small deformations our findings apply to any

isotropic, linear elastic material.

We note that when the size of inclusions is allowed to equilibrate through the exchange of mass via an evaporation–condensation process, the equilibrium size  $R$  can be calculated using classical nucleation theory augmented with an elasticity term [3, 19]. Surface tension favors large  $R$ , while elastic pressure favors small  $R$ . Competition between these two terms results in a well-defined equilibrium size.

### III. SIMULATIONS OF VISCOELASTIC RIPENING

Having described the (reversible) elastic response we emphasize that understanding the phase separation process requires a model of irreversible deformations. The simplest description of a material that is elastic on short time scales but can flow on long time scales is a Maxwell material, which is characterized by a single relaxation time  $\tau_r$ . For example, supramolecular networks [7] and vitrimers [27, 28], but also covalently cross-linked polymers [29], exhibit Maxwell-type viscoelastic relaxation on sufficiently long timescales. Moreover, both crystalline and amorphous materials are generally subject to diffusion creep that follows a single timescale relaxation process. In contrast, biopolymer networks [30], protein condensates [16] and glassy materials [31] exhibit aging and relaxation over multiple timescales and are instead described by a Maxwell glass model. For example, the strain  $\varepsilon$  of cytoskeleton under stress  $\sigma$  increases as a power law,  $\varepsilon \sim \sigma t^a$ , with exponent  $a \approx 0.5$  found both theoretically [32] and experimentally [33].

Coarsening processes are usually modeled using continuum mean-field theories [1], which very accurately predict growth laws in the large-domain and the long-time limits. We will develop such a theory in the next section. Modeling of small clusters on short timescales, however, requires a more detailed model that is able to accurately capture the interplay between nucleation, phase separation and viscoelastic relaxation. To this end, we first employ a Lennard-Jones (LJ) fluid as a prototypical particle-based model and couple it to a viscoelastic background medium with embedded spherical cavities (see Methods section). For a Maxwell material at constant strain, the elastic stress  $\sigma$  decays exponentially,  $\partial\sigma/\partial t = -\sigma/\tau_r$ , on a timescale  $\tau_r = \eta/E_Y$ , with  $\eta$  the material viscosity. This model assumes linear elasticity and small deformations and applying it directly to Eq. (1) could lead to unphysical behavior at large  $\lambda$ , where a small reduction in stress would imply an unphysically large change in strain. To avoid this artifact, we use a generalized form based on the reduction of the elastic energy  $E_{el}$ ,

$$\frac{\partial E_{el}}{\partial t} = -2 \frac{E_{el}}{\tau_r}, \quad (2)$$

which in the linear elasticity regime corresponds exactly

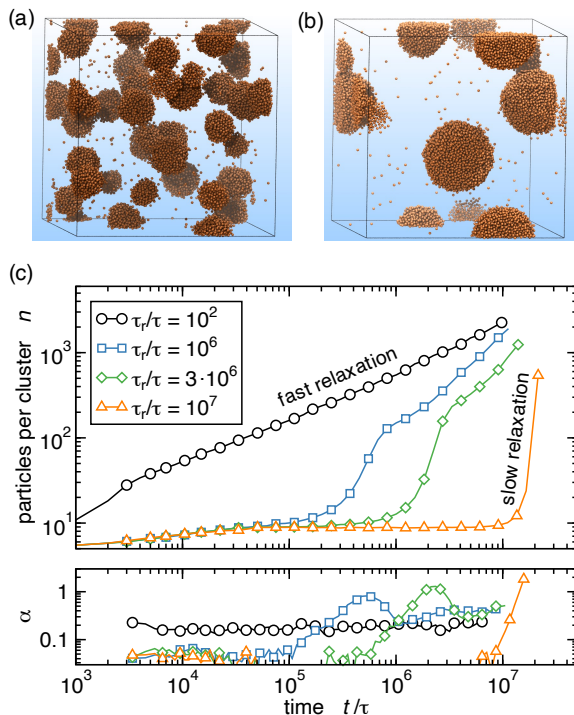


FIG. 2. Growth of condensates in a viscoelastic medium with relaxation time  $\tau_r$  as determined by Monte Carlo simulations. (a,b) Snapshots at times  $t = 8 \cdot 10^5 \tau$  (a) and  $t = 10^7 \tau$  (b) for  $\tau_r = 10^6 \tau$ . Individual spherical particles with diameter  $d_{LJ}$  are shown as orange spheres and the box outline indicates periodic boundaries. (c) Top panel: Growth in the average number of particles per cluster  $n$  for various  $\tau_r$ . Bottom panel: Ripening exponent  $\alpha$  [(Eq. (3))], which equals  $1/3$  of the slope in the top panel, since  $n \sim \bar{R}^3$ . Elastic parameters:  $E_Y = k_B T / d_{LJ}^3$  and  $E_c = 1$ .

to the Maxwell model.

The interplay of condensation and viscoelastic relaxation leads to specific dynamics of domain coarsening and cluster growth (Fig. 2), which we characterize via the growth exponent,

$$\alpha = \frac{d \log \bar{R}}{d \log t}, \quad (3)$$

with  $\bar{R}$  the mean cluster radius. Under sufficiently fast relaxation ( $\tau_r \rightarrow 0$ ), elasticity is irrelevant and the domain growth is expected to be determined by Ostwald ripening with a power-law exponent  $\alpha = 1/3$  in the large-domain limit [1, 34]. In our particle-based simulations we find  $\alpha \approx 0.23$  (Fig. 2c, bottom panel). This underestimation is a finite-size effect originating from the surface diffusion of individual particles [35]. However, if the viscoelastic medium relaxes more slowly, markedly different behavior results. On short timescales,  $t \ll \tau_r$ , the growth is limited and the evolution of cluster size is determined by elastic ripening [19], whereas on intermediate timescales,  $t \sim \tau_r$ , viscoelastic relaxation enables expansion of cavi-

ties and continued domain growth. Surprisingly, we discover that in this *viscoelastic ripening* regime the exponent exceeds the Ostwald value,  $\alpha > 1/3$ . Since the simulations are restricted to relatively small systems and limited timescales, we further explore the nature of this new regime, which is controlled by viscoelastic relaxation, by means of perturbation theory.

## IV. VISCOELASTIC RIPENING THEORY

### A. Extension of Landau–Slyozov–Wagner theory

The Landau–Slyozov–Wagner (LSW) theory of Ostwald ripening predicts that the average radius  $\bar{R}$  of a spherical domains grows as

$$\frac{d\bar{R}}{dt} = C c^{\text{sat}} \frac{\gamma}{\bar{R}^2}, \quad (4)$$

where  $c^{\text{sat}}$  is the monomer concentration in phase B,  $\gamma$  the surface tension and  $C$  the prefactor. The resulting power law-growth  $\bar{R} \sim t^{1/3}$ , is accompanied by a scale-free size distribution  $\psi(R/\bar{R})$  [1, 34, 36].

Elastic effects alter this coarsening process in two ways. Firstly, they change the phase equilibrium between the condensed phase (A) and the viscoelastic phase (B), which is captured by an elasticity-dependent  $c^{\text{sat}}$  [19]. Assuming that the monomers in phase B are dilute and can be described by the ideal chemical potential, we find

$$c^{\text{sat}}(p_{\text{el}}) = c_0^{\text{sat}} e^{p_{\text{el}} / (c_A k_B T)}, \quad (5)$$

with the elasticity-free reference value  $c_0^{\text{sat}} = c^{\text{sat}}(p_{\text{el}} \rightarrow 0)$  and  $c_A$  the monomer number density in the condensed phase A. Secondly, the elastic energy alters the coarsening kinetics. We account for this effect using a first-order perturbation expansion of the LSW theory (see Methods section), leading to the coarsening rate

$$\frac{d\bar{R}}{dt} = C c^{\text{sat}}(p_{\text{el}}) \left[ \frac{\gamma}{\bar{R}^2} - \frac{1}{4\pi} \frac{\partial [E_{\text{el}}(\bar{R}, \bar{r}) / \bar{R}^3]}{\partial \bar{R}} \right]. \quad (6)$$

The elastic pressure  $p_{\text{el}}$ , the average domain radius  $\bar{R}$  and the mean cavity radius  $\bar{r}$  are all time dependent, while the pre-factor  $C$  is determined by the diffusion constant  $D$  and the density of the condensed phase  $c_A$  [1]. We assume the limit in which the condensed phase A is incompressible relative to the surrounding viscoelastic phase B, and thus both  $c_A$  and  $C$  are considered constant. The surface tension  $\gamma$  is positive, while the elastic term in Eq. (6) can be either positive or negative and thus can either accelerate or inhibit the coarsening. For example, the extended Gent model leads to growth in  $\bar{R}$  until the elastic term balances the surface tension term, at which point the growth is arrested and  $\bar{R}$  exponentially approaches its equilibrium value. Equation (6) predicts coarsening kinetics and qualitatively explains experimental data for elastic ripening [3, 19], whereas in the absence of elasticity,  $E_{\text{el}} = 0$ , it reduces to the LSW theory, Eq. (4).

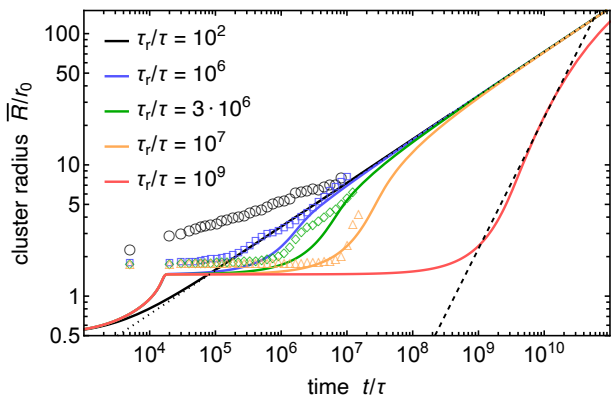


FIG. 3. Theoretical prediction for cluster growth obtained by numerical integration of Eqs. (2) and (6) (solid lines), with corresponding MC simulation results for different relaxation times,  $\tau_r/\tau = 10^2$  (circles),  $\tau_r/\tau = 10^6$  (squares),  $\tau_r/\tau = 3 \cdot 10^6$  (diamonds) and  $\tau_r/\tau = 10^7$  (triangles). The dotted black line shows the LSW theory prediction, Eq. (4), and the dashed line is the small deformation approximation to viscoelastic ripening, Eq. (8). Initial cavity diameter  $r_0 = d_{LJ}$  and  $E_Y = k_B T / r_0^3$ .

To model viscoelastic relaxation, we couple Eq. (6) with a description of cavity expansion,  $d\bar{r}/dt$ , determined from Eq. (2) (see Supplemental Material). The two coupled differential equations are integrated numerically providing a prediction for domain growth (Fig. 3). Strikingly, our extension of LSW theory qualitatively captures the observations of Sec. III. In particular, we note that the perturbative solution confirms the existence of the intermediate viscoelastic ripening regime where the growth exponent,  $\alpha \sim 1$ , exceeds that of Ostwald ripening ( $\alpha \sim 1/3$ ).

To directly compare the theory to the results of Fig. 2, we determine the prefactor  $C = 8D/(27c_A^2 k_B T)$  [1, 34], with  $D$  the diffusion coefficient, from the MC simulation conditions (see Methods section). Given the first-order nature of the theory, the semi-quantitative agreement with the MC data is quite remarkable (Fig. 3). Moreover, deviations at small  $\bar{R}$  are to be expected, since LSW theory is only valid in the large-domain limit. Conversely, we note that the simulation results for the longest times exhibit quantitative agreement with the theoretical predictions. Similar agreement is observed for materials that support elastic cavitation (see Supplemental Material). Lastly, we note that the theory illustrates how viscoelastic effects can change the predicted domain size by orders of magnitude.

## B. Analytical theory

Whereas the perturbative solution resolves the cluster growth process across all time scales, an analytical theory would describe the viscoelastic ripening regime without the need for a numerical solution. Here we derive such a

theory by assuming a small expansion ratio,  $\lambda \approx 1$ . In this case, the elastic term in Eq. (6) simplifies to  $\sigma/\bar{R}$ , with  $\sigma$  the radial stress. Under elastic arrest,  $d\bar{R}/dt \approx 0$ , the stress is thus determined solely by the surface tension,

$$\sigma \approx \gamma/\bar{R}. \quad (7)$$

We note that this approximation did not require linear elasticity assumptions. The same relation can be obtained by employing classical nucleation theory and assuming quasi-equilibrium conditions for a system of spherical clusters at a constant total volume (see Supplemental Material). Combining Eq. (2), which reduces to  $d\bar{r}/dt = (\lambda - 1)\bar{r}/\tau_r$ , with Eq. (7) and the linear elastic stress,  $\sigma = 2\tilde{E}_Y(\lambda - 1)$  [26], where  $\tilde{E}_Y = E_Y/(1 + \nu)$ , results in an analytical prediction for the growth rate,

$$\frac{d\bar{R}}{dt} = \frac{\gamma}{2\tau_r \tilde{E}_Y}. \quad (8)$$

This expression is in excellent agreement with the numerical integration result in the viscoelastic ripening regime with exponent  $\alpha = 1$  (dashed line in Fig. 3). Interestingly, the same expression is found for late-stage coarsening in spinodal decomposition of inter-percolating phases [5, 6], but the underlying mechanism is different. Whereas we consider an evaporation-condensation process at intermediate timescales, the coarsening of inter-percolating networks is a result of hydrodynamic flow on long timescales. Surprisingly, both cases lead to the same coarsening law, Eq. (8).

The extent of the viscoelastic ripening regime is limited by monomer diffusion, with a typical diffusion timescale  $\tau_D = \bar{R}^2/D$ , and a transition to Ostwald ripening occurs at sufficiently large cluster size  $R_c$  (Fig. 3). To determine the crossover size  $R_c$ , we equate the two growth rates, Eqs. (4) and (8),

$$R_c^2 = \frac{16c^{\text{sat}}}{27c_A^2} \frac{D\tau_r \tilde{E}_Y}{k_B T}. \quad (9)$$

Viscoelastic ripening is limited to  $\bar{R} < R_c$  and will thus be prominent if  $D\tau_r$  is large, with  $\tau_r$  the Maxwell relaxation time. In a single-component phase, these two factors are connected via the fluctuation-dissipation theorem. Employing the Stokes-Einstein relation and assuming a standard situation with a dense phase A, i.e.,  $c_A \sim r_m^{-3}$  with  $r_m$  the molecular size of individual monomers, we find  $R_c < r_m$ , so that viscoelastic ripening does not exist [37]. We conclude that viscoelastic ripening of precipitates or liquid droplets is expected to occur only in multicomponent materials that can simultaneously support both fast diffusion of monomers and sufficiently slow material relaxation. A typical example of such material is a hydrogel.

To quantitatively delineate the different growth regimes, we consider that the viscoelastic growth, Eq. (8), is noticeable upon doubling of the initial cluster size,

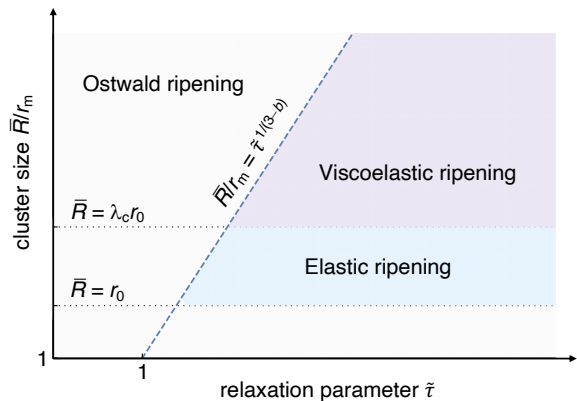


FIG. 4. Theoretical diagram delineating the domain growth regimes in a general viscoelastic material on a double-logarithmic scale: Ostwald ripening (light grey), elastic (light blue) and viscoelastic ripening (light purple). The boundaries are determined by the initial cavity size  $r_0$  (lower dotted line), the reversible elastic (cavitation) expansion  $\lambda_c$  (upper dotted line) and the crossover to Ostwald ripening (dashed line) as a function of the relaxation parameter  $\tilde{\tau}$ , Eq. (15). For a Maxwell material,  $a = 1$  and  $b = 1$ , the crossover is given by Eq. (9) and the relaxation parameter becomes proportional to the Maxwell relaxation time,  $\tilde{\tau} \propto \tau_r$ .

which occurs on a time scale  $\tau_{ve}$ ,

$$\tau_{ve} = \tau_r \frac{2\tilde{E}_Y r_0}{\gamma}, \quad (10)$$

whereas the transition to Ostwald ripening occurs at crossover time scale  $\tau_c$  determined by Eqs. (8) and (9),

$$\tau_c = \tau_{ve} \frac{4}{c_A r_0} \sqrt{\frac{D c_{sat} \tau_r \tilde{E}_Y}{27 k_B T}}. \quad (11)$$

Thus, the distinct ripening regimes are characterized as: (i) initial growth and elastic arrest for  $t < \tau_{ve}$ ; (ii) viscoelastic ripening with growth exponent  $\alpha \approx 1$  for  $\tau_{ve} < t < \tau_c$ ; and (iii) convergence to the LSW theory with  $\alpha \approx 1/3$  for  $t > \tau_c$ .

### C. Power-law material response

The accuracy of the analytical prediction shows that our approach can be generalized to any relaxation behavior with a strain rate that is a power-law function of both the stress  $\sigma$  and time  $t$ ,

$$\frac{d\varepsilon}{dt} = A \sigma^b t^{a-1}, \quad (12)$$

with  $A$  a materials-dependent prefactor. This general form captures power-law fluids as well as a variety of glassy materials and networks [31]. Setting the exponents  $a$  and  $b$  both to unity and  $A$  to  $(2\tilde{E}_Y \tau_r)^{-1}$  would correspond to the Maxwell material analyzed above, whereas

for the cytoskeleton  $a = 0.5$  and  $b = 1$  [32, 33]. Under viscoelasticity-limited growth, Eq. (7), and small strains,  $\varepsilon = \lambda - 1 \sim 0$ , we find  $d\bar{R}/dt = A\gamma^b \bar{R}^{1-b} t^{a-1}$ , which can be analytically integrated to obtain the general growth equation for viscoelastic ripening,

$$\bar{R}(t)^b = \gamma^b \frac{Ab}{a} t^a. \quad (13)$$

This growth regime is limited by the minimum cavity size  $r_0$  and the transition to the Ostwald ripening regime at the crossover size,

$$R_c(t) = r_m \tilde{\tau}^{\frac{1}{3-b}}, \quad (14)$$

obtained by equating the LSW and viscoelastic growth rates, with the dimensionless relaxation parameter

$$\tilde{\tau} = \frac{8Dc_{sat}\gamma^{1-b}t^{1-a}}{27Ac_A^2 k_B T r_m^{3-b}}. \quad (15)$$

If the initial elastic expansion of cavities is significant,  $\lambda_c \gg 1$ , we can also delineate a purely elastic ripening regime,  $r_0 < \bar{R} < \lambda_c r_0$ , that does not depend on relaxation properties [19]. Figure 4 summarizes the growth regimes [38]. Interestingly, for a strongly shear-thinning material the behavior becomes qualitatively different from a Maxwell material. At  $b > 3$  the slope of the boundary in Fig. 4 turns negative; small clusters are limited by Ostwald ripening, while larger domains fall into the viscoelastic ripening regime.

Having extensively analyzed viscoelastic relaxation, we note that the viscoelastic matrix could form a brittle crack if the elastic stress exceeds the fracture strength  $p_{\text{frac}} = \sqrt{E_Y \Gamma / R}$  and  $R \geq \Gamma / E_Y$ , with  $\Gamma$  the fracture energy of the material [4]. We find the elastic stress that can be produced by surface tension-driven domain growth is limited to  $p_{\text{el}} \sim \gamma / R$ , Eq. (7). Thus, formation of a brittle crack would require the surface tension to exceed the fracture energy,  $\gamma > \Gamma$ . However, since surface tension is typically orders of magnitude smaller than the fracture energy [4], we conclude that viscoelastic relaxation is the dominant out-of-equilibrium process leading to stress relaxation in surface-tension driven coarsening.

## V. CONCLUSIONS

We have addressed the problem of phase separation within a viscoelastic material, a question of fundamental importance to different classes of soft materials. Through a combination of analytical calculations and Monte Carlo simulation, we have demonstrated that such systems can exhibit a new type of domain ripening behavior that is distinct from the standard Ostwald ripening process. Our analytical results, supported by MC simulations, show that ripening of phase-separated domains typically exhibits three distinct regimes: (i) elastic ripening and arrest on short timescales; (ii) viscoelastic ripening on in-



intermediate timescales with a material-dependent ripening exponent  $\alpha$ , e.g.,  $\alpha \sim 1$  for a Maxwell material; and (iii) Ostwald ripening with  $\alpha = 1/3$  in the long time limit.

These findings provide insight into phase separation within a wide variety of viscoelastic materials, including dense polymer solutions, gels and biological networks like the cytoskeleton. Whereas covalently cross-linked gels or glassy plastics at room temperature exhibit only marginal viscoelastic relaxation, many materials exhibit creep flow and thus domain growth is possible on sufficiently long timescales of years or even centuries [29]. Thus, our findings may have implications for predicting the aging and long-term stability of materials, and could explain the phase separation and coarsening observed in old oil paintings [12].

Interestingly, our results suggest that cells could regulate the domain size of membrane-less organelles [13] by controlling the viscoelastic properties of the surrounding cytoskeleton network. Whereas the present work focuses on passive, surface-tension-driven phase separation, qualitatively different ripening regimes could emerge if condensation and growth are driven by active processes [39]. Our perturbation approach offers an avenue to explore such driven systems.

Lastly, we note that the framework presented can be applied to both fluid and solid spheroidal inclusions, since the stress inside solid spheroidal inclusions is constant [40]. Although crystalline precipitates are often faceted [4], for a compact, convex inclusion the required corrections are expected to be small [26], so that our framework qualitatively applies to crystalline inclusions as well.

## VI. METHODS

### A. Monte Carlo simulations

The simulated system comprises  $N_p = 25000$  particles suspended in an implicit solvent and placed in a periodic cubic box of linear size  $L = 70d_{LJ}$ . The pair interaction between particles of diameter  $d_{LJ}$  and center-to-center distance  $d_{ij}$  is modeled via a Lennard-Jones (LJ) potential  $U_{LJ}(d_{ij})$  with cut-off  $2.5d_{LJ}$  and interaction strength  $\epsilon_{LJ}$ . To preserve the appropriate diffusion dynamics of individual particles, we only use local MC moves, consisting of a random displacement of a single particle to a position within a sphere of radius  $d_{LJ}/2$ , centered on the original position of the particle. The simulation timescale  $\tau = d_{LJ}^2/40D$  is thus defined by the size of the particles and their diffusion constant  $D$ .

This standard LJ system is coupled to a viscoelastic background medium with embedded spherical cavities. Every cluster containing two or more particles is considered to be in phase A and is subject to elastic stress, whereas isolated particles are considered to be in phase B and are not subject to elastic stress. When a dimer (a two-particle cluster) forms, a cavity with initial radius  $r_0$

is created at  $\mathbf{r}_{cav}$ , the center of mass of the two particles. This position remains fixed as the cluster grows, unless the cluster fully dissolves into individual particles, at which point the memory of the cavity location disappears. The elastic energy of the cavity is determined by the mismatch between the radii of the cluster  $R$  and of the cavity  $r$ . Viscoelastic relaxation effects are modeled via dissipative expansion of cavities. The cavity growth rate  $\dot{r}$  is obtained from the relaxation of the elastic energy (see Supplemental Material). Cavities are expanded after each MC cycle of  $N_p$  attempted displacement moves via  $r \rightarrow r + \tau\dot{r}$ .

To calculate the elastic energy we assume a dilute situation in which individual clusters  $k$  of particles do not interact through elastic deformations of the surrounding medium and the elastic energy of the system is given by the sum of individual cluster contributions  $E_{el,k}$ . The total energy of the system is thus

$$E = \sum_{i,j} U_{LJ}(d_{ij}) + \sum_k E_{el,k}, \quad (16)$$

where the first sum is performed over all pairs of particles and the second sum over all clusters. To compute the location and position of the clusters we use a neighbor-based cluster identification algorithm. Two particles are considered neighbors (and thus belong to the same cluster) if their center-to-center distance is less than  $1.5d_{LJ}$ . Each cluster is characterized by its center-of-mass position  $\mathbf{r}_k$  and radius of gyration  $r_{g,k}$ . Since isolated clusters attain a spherical shape with radius  $R_k = r_{g,k}\sqrt{5/3}$ , the coupling with the elastic medium depends only on  $r_{g,k}$  and  $\mathbf{r}_k$ . The elastic energy due to cavity expansion is obtained by integrating the elastic pressure,  $E_{ex} = \int_r^R 4\pi(r')^2 p_{el}(r'/r) dr'$  for  $R > r$ , and  $E_{ex} = 0$  otherwise. To represent the displacement  $d = |\mathbf{r} - \mathbf{r}_{cav}|$  of the center of mass  $\mathbf{r}$  of the cluster with respect to the cavity position  $\mathbf{r}_{cav}$ , we add a linear elastic displacement term  $E_d = \pi E_Y R d^2$  for  $R > r + d$  and  $E_d = 0$  otherwise [26]. The total elastic energy,  $E_{el} = E_{ex} + E_d$ , both suppresses the growth and immobilizes the clusters. No pinning of clusters to cavity walls is considered, i.e., partially filled cavities are allowed and do not provide additional free-energy contributions.

Phase equilibrium is determined by the LJ interaction parameter  $\epsilon_{LJ}$  and the density  $\rho = N_p/L^3$ , while the viscoelastic properties are determined by the modulus  $E_Y$ , the coefficient  $E_c$ , and the viscoelastic relaxation time relative to the diffusion timescale  $\tau_r/\tau$ . The calculations are performed at temperature  $T = \epsilon_{LJ}/(1.8k_B)$ , which is in a two-phase coexistence region of the LJ phase diagram (cf. Fig. 2a,b and Supplemental Material for supporting data at higher temperatures). We set  $E_Y = k_B T/d_{LJ}^3$  and  $r_0 = d_{LJ}$ , corresponding to a flexible gel with crosslink distance  $r_0 = d_{LJ}$  [20]. The average cluster size  $n$  and radius  $\bar{R}$  are obtained by a system average of all clusters with more than 5 particles, to avoid counting transient small aggregates. Mapping between simulation and theoretical parameters is obtained

from equilibrium properties of the LJ fluid [41] and the simulation timescale.

## B. Perturbation theory

We consider viscoelastic effects in a first-order perturbative expansion of the LSW Ostwald ripening theory, Eq. (4). For clarity we use dot-notation for derivatives,  $\dot{R} \equiv dR/dt$ . The growth rate of the mean cluster size  $\dot{\bar{R}}$  depends on the thermodynamic driving force  $f$  and the kinetic prefactors, such as the diffusion constant, which determine monomer transport. Here we assume that monomers can diffuse uninhibited through the viscoelastic medium, so that the kinetic prefactors are constant.

The first-order correction to LSW ripening due to viscoelastic effects is

$$\dot{\bar{R}} = \dot{\bar{R}}_0 + \left. \frac{\partial \dot{\bar{R}}}{\partial f} \right|_0 (f - f_0), \quad (17)$$

where  $f_0$  is the driving force in reference (LSW) system, which only depends on the surface tension, and the derivative is evaluated in this reference system. Within this first-order expansion the relative cluster size distribution  $\psi(R/\bar{R})$  is assumed to remain constant (see Supplemental Material). The approximation thus depends

solely on the viscoelastic contribution to the thermodynamic driving force, which is given by the derivative of the free-energy density,

$$f = - \left. \frac{\partial(F/V)}{\partial \bar{R}} \right|_V, \quad (18)$$

at constant total volume  $V$  of  $N$  spherical clusters in the system. The free energy is determined by the surface tension and elastic energy contributions,

$$F = \sum_i [4\pi\gamma R_i^2 + E_{\text{el}}(R_i, r_i)], \quad (19)$$

summed over all clusters in the system. Applying the mean-field approximation,  $F = NF_1(\bar{R}, \bar{r})$ , with  $F_1(\bar{R}, \bar{r})$  the free energy of the average cluster, we obtain the first-order perturbative correction to the LSW theory, Eq. (6).

## ACKNOWLEDGMENTS

We thank Peter Voorhees, Eric Dufresne and Robert Style for enlightening discussions. This work was supported by the E.U. Horizon 2020 program under the Marie Skłodowska-Curie fellowship No. 845032, the U.S. National Science Foundation through Grant No. DMR-1610796 and the Center for Scientific Studies in the Arts at Northwestern University, which is funded by the Andrew W. Mellon Foundation.

- 
- [1] L. Ratke and P. W. Voorhees, Nucleation, growth and coarsening, in *Growth and Coarsening: Ostwald Ripening in Material Processing* (Springer, Berlin, 2002) pp. 205–224.
  - [2] F. R. N. Nabarro, The strains produced by precipitation in alloys, Proc. R. Soc. London, Ser. A **175**, 519 (1940).
  - [3] R. W. Style, T. Sai, N. Fanelli, M. Ijavi, K. Smith-Mannschott, Q. Xu, L. A. Wilen, and E. R. Dufresne, Liquid-liquid phase separation in an elastic network, Phys. Rev. X **8**, 011028 (2018).
  - [4] J. Y. Kim, Z. Liu, B. M. Weon, T. Cohen, C.-Y. Hui, E. R. Dufresne, and R. W. Style, Extreme cavity expansion in soft solids: Damage without fracture, Sci. Adv. **6** (2020).
  - [5] E. D. Siggia, Late stages of spinodal decomposition in binary mixtures, Phys. Rev. A **20**, 595 (1979).
  - [6] H. Tanaka, Viscoelastic phase separation, J. Phys.: Condens. Matter **12**, R207 (2000).
  - [7] H. Tabuteau, S. Mora, G. Porte, M. Abkarian, and C. Ligoure, Microscopic mechanisms of the brittleness of viscoelastic fluids, Phys. Rev. Lett. **102**, 155501 (2009).
  - [8] R. Pascova, I. Gutzow, and J. Schmelzer, A model investigation of the process of phase formation in photochromic glasses, J. Mater. Sci. **25**, 921 (1990).
  - [9] J. Schmelzer, I. Gutzow, and R. Pascova, Kinetics of phase segregation in elastic and viscoelastic media, J. Cryst. Growth **104**, 505 (1990).
  - [10] J. W. P. Schmelzer, R. Müller, J. Möller, and I. S. Gutzow, Theory of nucleation in viscoelastic media: application to phase formation in glassforming melts, J. Non-Cryst. Solids **315**, 144 (2003).
  - [11] H. Tanaka, T. Araki, T. Koyama, and Y. Nishikawa, Universality of viscoelastic phase separation in soft matter, J. Phys.: Condens. Matter **17**, S3195 (2005).
  - [12] F. Casadio, K. Keune, P. Noble, A. van Loon, E. Hendriks, S. A. Centeno, and G. Osmond, eds., *Metal Soaps in Art: Conservation and Research* (Springer, 2019).
  - [13] M. Feric, N. Vaidya, T. S. Harmon, D. M. Mitrea, L. Zhu, T. M. Richardson, R. W. Kriwacki, R. V. Pappu, and C. P. Brangwynne, Coexisting liquid phases underlie nucleolar subcompartments, Cell **165**, 1686 (2016).
  - [14] S. Alberti, A. Gladfelter, and T. Mittag, Considerations and challenges in studying liquid-liquid phase separation and biomolecular condensates, Cell **176**, 419 (2019).
  - [15] S. C. Weber, Sequence-encoded material properties dictate the structure and function of nuclear bodies, Curr. Opin. Cell Biol. **46**, 62 (2017).
  - [16] L. Jawerth, E. Fischer-Friedrich, S. Saha, J. Wang, T. Franzmann, X. Zhang, J. Sachweh, M. Ruer, M. Ijavi, S. Saha, J. Mahamid, A. A. Hyman, and F. Jülicher, Protein condensates as aging Maxwell fluids, Science **370**, 1317 (2020).
  - [17] Y. Shin, Y.-C. Chang, D. S. W. Lee, J. Berry, D. W. Sanders, P. Ronceray, N. S. Wingreen, M. Haataja, and

- C. P. Brangwynne, Liquid nuclear condensates mechanically sense and restructure the genome, *Cell* **175**, 1481 (2018).
- [18] D. S. W. Lee, N. S. Wingreen, and C. P. Brangwynne, Chromatin mechanics dictates subdiffusion and coarsening dynamics of embedded condensates, *Nature Phys.* **17**, 531 (2021).
- [19] K. A. Rosowski, T. Sai, E. Vidal-Henriquez, D. Zwicker, R. W. Style, and E. R. Dufresne, Elastic ripening and inhibition of liquid–liquid phase separation, *Nature Phys.* **16**, 422 (2020).
- [20] M. Rubinstein and R. H. Colby, *Polymer Physics* (Oxford University Press, Oxford, 2003).
- [21] A. N. Gent and C. Wang, Fracture mechanics and cavitation in rubber-like solids, *J. Mater. Sci.* **26**, 3392 (1991).
- [22] A. N. Gent, A new constitutive relation for rubber, *Rubber Chem. Technol.* **69**, 59 (1996).
- [23] J. A. Zimmerman, N. Sanabria-DeLong, G. N. Tew, and A. J. Crosby, Cavitation rheology for soft materials, *Soft Matt.* **3**, 763 (2007).
- [24] S. B. Hutchens, S. Fakhouri, and A. J. Crosby, Elastic cavitation and fracture *via* injection, *Soft Matt.* **12**, 2557 (2016).
- [25] The exact expression for  $p_{\text{el}}^{\text{lim}}$  is not of crucial importance. Any functional form that limits the expansion ratio,  $p_{\text{el}}^{\text{lim}} \sim \lambda^\kappa$  as  $\lambda \rightarrow \infty$ , with  $\kappa > 0$ , could be used.
- [26] L. D. Landau and E. M. Lifshitz, *Theory of Elasticity*, Course of Theoretical Physics, Vol. 3 (Pergamon, London, 1959).
- [27] W. Denissen, M. Droesbeke, R. Nicolaÿ, L. Leibler, J. M. Winne, and F. E. Du Prez, Chemical control of the viscoelastic properties of vinylogous urethane vitrimers, *Nature Comm.* **8**, 14857 (2017).
- [28] B. M. El-Zaatari, J. S. A. Ishibashi, and J. A. Kalow, Cross-linker control of vitrimer flow, *Polym. Chem.* **11**, 5339 (2020).
- [29] G. Capiel, E. Hernández, N. E. Marcovich, and M. A. Mosiewicki, Stress relaxation behavior of weldable crosslinked polymers based on methacrylated oleic and lauric acids, *Eur. Polym. J.* **132**, 109740 (2020).
- [30] Y. Mulla, F. C. MacKintosh, and G. H. Koenderink, Origin of slow stress relaxation in the cytoskeleton, *Phys. Rev. Lett.* **122**, 218102 (2019).
- [31] P. Sollich, F. Lequeux, P. Hébraud, and M. E. Cates, Rheology of soft glassy materials, *Phys. Rev. Lett.* **78**, 2020 (1997).
- [32] C. P. Broedersz, M. Depken, N. Y. Yao, M. R. Pollak, D. A. Weitz, and F. C. MacKintosh, Cross-link-governed dynamics of biopolymer networks, *Phys. Rev. Lett.* **105**, 238101 (2010).
- [33] N. Desprat, A. Richert, J. Simeon, and A. Asnacios, Creep function of a single living cell, *Biophys. J.* **88**, 2224 (2005).
- [34] A. Baldan, Progress in Ostwald ripening theories and their applications to nickel-base superalloys. Part I: Ostwald ripening theories, *J. Mater. Sci.* **7**, 2171 (2002).
- [35] C. Jeppesen and O. G. Mouritsen, Universality of ordering dynamics in conserved multicomponent systems, *Phys. Rev. B* **47**, 14724 (1993).
- [36] I. M. Lifshitz and V. V. Slyozov, The kinetics of precipitation from supersaturated solid solutions, *J. Phys. Chem. Solids* **19**, 35 (1961).
- [37] Viscoelastic ripening could potentially be found in a one-component system provided  $c_A \ll r_m^{-3}$ , which would occur if gas bubbles nucleate within a dense phase and grow via surface-tension driven coarsening.
- [38] This figure does not cover the case in which initial nucleation and growth of small clusters follows a  $R \sim t^2$  scaling [1].
- [39] D. Zwicker, R. Seyboldt, C. A. Weber, A. A. Hyman, and F. Jülicher, Growth and division of active droplets provides a model for protocells, *Nature Phys.* **13**, 408 (2017).
- [40] J. D. Eshelby, The determination of the elastic field of an ellipsoidal inclusion, and related problems, *Proc. R. Soc. London, Ser. A* **241**, 376 (1957).
- [41] J. Janeček, Long range corrections in inhomogeneous simulations, *J. Phys. Chem. B* **110**, 6264 (2006).